Structure and Function of YcnD from *Bacillus subtilis,* a Flavin-Containing Oxidoreductase[†,‡]

Alexander Morokutti,[§] Andrzej Lyskowski,[||] Sonja Sollner,[§] Eva Pointner,[§] Teresa B. Fitzpatrick,[⊥] Christoph Kratky,[||] Karl Gruber,*[,||,#] and Peter Macheroux*[,§]

Institut für Biochemie, Technische Universität Graz, Institut für Chemie, Karl-Franzens Universität Graz, Institut für Pflanzenwissenschaften, Eidgenössische Technische Hochschule Zürich, and Research Center Applied Biocatalysis, A-8010 Graz, Austria

Received June 7, 2005; Revised Manuscript Received August 23, 2005

ABSTRACT: YcnD from the Gram-positive bacterium *Bacillus subtilis* is a member of a family of bacterial proteins that act as NADH- and/or NADPH-dependent oxidoreductases. Here, we report for the first time on the biochemical characterization of the purified protein, demonstrating that YcnD is an FMN-containing enzyme that can be reduced by NADH or NADPH (K_m = 6.4 and 4.4 μM, respectively). In the presence of free FMN as the electron-accepting substrate, the latter reductant showed a ping-pong Bi-Bi reaction mechanism, whereas utilization of NADH is competitively inhibited by this substrate. This finding suggests that NADPH is the physiological reductant of the enzyme. We also show that YcnD reduces nitro-organic compounds, chromate, and a series of azo dyes. The reduction of azo dyes appears to be mediated by free reduced FMN because the reaction is considerably slower in its absence. Structure determination by X-ray crystallography revealed that YcnD folds into a three layer $\alpha-\beta-\alpha$ sandwich strongly resembling the topology of the NADH oxidase superfamily. Similar to homologous bacterial oxidoreductase, YcnD forms homodimers with an extended dimer interface. The biochemical data and the structure are discussed in light of the putative physiological function of YcnD as an oxidoreductase delivering reduced FMN to enzymes that require the reduced cofactor for activity.

The generation of complete genome sequences has produced vast information on the proteins of several pro- and eukaryotic species. However, the function of the proteins can often be inferred only by sequence similarity to proteins that were characterized biochemically from other sources. In the Gram-positive bacterium *Bacillus subtilis*, a large fraction of proteins (42%) could not be assigned a functional role and, therefore, were annotated as hypothetical proteins of unknown function (*1*). Among these functionally unassigned proteins is a family of enzymes that are proposed to act as NAD(P)H-dependent flavin oxidoreductases (ORs).[1] The family comprises YcnD (also termed NfrA2), YwcG (NfrA1), YdfN, YdgI, and YodC. The first two proteins, YcnD and YwcG, are identical in length (249 amino acids) and are phylogenetically closely related to each other. YwcG has been shown to reduce nitro compounds as well as free flavin (*2*). The latter activity can be understood in a physiological context because there are several cellular functions for reduced FMN.

First, reduced flavin can directly mediate electron transfer to ferric complexes or iron-containing enzymes such as the iron center of ribonucleotide reductase (*3*), or second, free reduced flavin (in the form of $FMNH_2$ or $FADH_2$) can bind to enzymes that have an absolute requirement for a reduced flavin cofactor for activity. These enzymes can be subdivided into two major groups: (i) flavin-dependent hydroxylases (monooxygenases), where the reduced flavin cofactor is consumed stoichiometrically during substrate turnover, and (ii) flavoenzymes, where acquisition of the reduced cofactor supports multiple substrate turnover because the catalyzed reaction is redox-neutral.

Typically, flavin-dependent hydroxylases utilize NADH or NADPH to reduce the tightly bound FMN or FAD cofactor and are therefore also termed "bifunctional". In contrast to these enzymes, there is also a group of the monofunctional hydroxylases, which depend upon an external source of reduced FAD to carry out hydroxylation of the substrate and comprise most of the first group (i) of enzymes mentioned above. A comprehensive review of these hydroxylases can be found in ref *4*. In addition to classical hydroxylases, group (i) also contains a very unusual bacterial enzyme, luciferase. In the luciferase-catalyzed reaction, reduced FMN reacts with dioxygen to form a 4a-hydroperoxide, which then oxidizes a long-chain aldehyde (e.g.,

[†] This work was supported by the Austrian Fonds zur Förderung der wissenschaftlichen Forschung (FWF) to P.M. (P17471) and to C.K. (P17132).

[‡] The PDB accession code for the structure reported is 1ZCH.

* To whom correspondence should be addressed: Graz University of Technology, Institute of Biochemistry, Petersgasse 12/II, A-8010 Graz, Austria. Telephone: +43-316-873-6450. Fax: +43-316-873-6952. E-mail: peter.macheroux@tugraz.at (P.M.); Research Center Applied Biocatalysis Graz, c/o Institute of Chemistry, Heinrichstrasse 28, A-8010 Graz, Austria. Telephone: +43-316-380-5483. Fax: +43-316-380-9850. E-mail: karl.gruber@uni-graz.at (K.G.).

[§] Technische Universität Graz.

[||] Karl-Franzens Universität Graz.

[⊥] Eidgenössische Technische Hochschule Zürich.

[#] Research Center Applied Biocatalysis.

[1] Abbreviations: HEPES, 4-(2-hydroxyethyl)piperazine-1-ethanesulfonic acid; NBS, methyl-4-nitrobenzenesulfonate; NF, 5-nitro-2-furaldehyde semicarbazone; NP, 4-nitrophenol; PEG, poly(ethylene glycol); OR, oxidoreductase.

10.1021/bi0510835 CCC: $30.25
Published on Web 09/30/2005

decanal) to the corresponding fatty acid. Very unusual is the fact that this reaction is accompanied by the emission of light. Because the enzyme cannot generate the required reduced cofactor, luciferase depends upon the generation of reduced FMN by a flavin reductase. Clearly, association with such an enzyme would ensure a reliable supply of reduced flavin. In fact, complex formation between luciferase from the marine bioluminescent bacteria *Vibrio harveyi* and a NADPH:FMN OR could be demonstrated recently (*5*). This OR, flavin reductase P, belongs to a family of enzymes capable of interacting with the luciferase present in certain bioluminescent bacteria.

The second group of enzymes comprises enzymes such as chorismate synthase and DNA photolyase. The latter enzyme employs an excited-state reduced flavin for transient electron donation to cleave pyrimidine dimers, thereby restoring the integrity of DNA (*6*). Similarly, chorismate synthase, the seventh enzyme of the shikimate pathway, appears to employ the same strategy for the transformation of 5-enolpyruvylshikimate 3-phosphate to chorismate (*7*). According to the current model, the *anti*-1,4-elimination of the C-(6*proR*)-hydrogen and the 3-phosphate group is initiated by the transfer of an electron to the substrate leading to C−O and C−H bond cleavage followed by back-transfer of an electron to the flavin. Because both reactions are redox-neutral, the reduced flavin is not consumed during turnover. Therefore, uptake of the reduced cofactor is a one time event in the absence of a reoxidizing agent such as dissolved dioxygen. The source of $FADH_2$ and $FMNH_2$ for DNA photolyase and chorismate synthase, respectively, remains elusive, but it can be speculated that ORs are involved in a fashion similar to the case of the monofunctional hydroxylases, discussed above. In the case of *B. subtilis* chorismate synthase, a trimeric protein complex comprising 3-dehydroquinate synthase (the second enzyme of the shikimate pathway), chorismate synthase, and a NADPH:FMN OR was reported by Hasan and Nester (*8*). The authors demonstrated in this study that the OR was able to provide the required reduced FMN for chorismate synthase activity. However, because of the low stability and yield of the trimeric protein complex, the identity of the OR could not be elucidated. Interestingly, the *B. subtilis* genome contains two genes, *ycnD* and *ywcG*, which share a significant degree of similarity with the ORs reported to provide reduced FMN to bacterial luciferase (e.g., YcnD shows 34.6% identity to the flavin reductase from *V. harveyi*). For YwcG, it could even be shown that it supports the activity of bacterial luciferase, and a change in the kinetic mechanism suggests the formation of a protein−protein complex (*2*). Therefore, it is conceivable that the two homologous ORs in *B. subtilis* play a role in generating reduced flavin for enzymes requiring a supply for their enzymatic activity. To investigate the functional role of YcnD and YwcG, we have initiated the functional characterization of the proteins.

Here, we report the initial biochemical and structural characterization of YcnD. These studies demonstrate that YcnD is a flavin-containing protein capable of reducing a variety of molecules such as FMN, nitro-organic compounds, chromate and azo dyes at the expense of either NADH or NADPH. Kinetic measurements have been performed to characterize the enzyme mechanism and to determine substrate affinities. The biochemical study of the enzyme was complemented by the analysis of the three-dimensional structure of YcnD by X-ray crystallography.

MATERIALS AND METHODS

Reagents. All chemicals were of the highest grade commercially available and purchased from Sigma−Aldrich, Fluka, or Merck. The Ni-nitrilotriacetate (Ni-NTA) agarose was from Qiagen, and the HiTrap chelating column was from Pharmacia Biotech AB.

Cloning, Expression, and Purification of B. subtilis *YcnD.* The DNA sequence of the *ycnd* gene of *B. subtilis* strain 168 was obtained from SubtiList (http://genolizt.pasteur.fr/SubtiList/). The gene was amplified by the polymerase chain reaction from genomic DNA isolated as described in ref *9*, using the following primers: (5′, GGAATTCCATATGAATGAAGTGATTAAATCTTTAAC; 3′, ATAAGAATGCGGCCGCTTTTTCAACTTTAAATCCTTGTTTTTC) and inserted into the *Nde*I/*Not*I restriction sites of pET21a (Novagen) to create the expression construct pYcnD. Cloning into the vector in this way allows expression of the protein with a hexa-histidine affinity tag at the C terminus. The construct was verified by sequence analysis after transformation into *Escherichia coli* DH5α cells (Stratagene). For analysis of expression, the construct was transformed into *E. coli* BL21 (DE3) cells; a single transformant was grown overnight in 5 mL of Luria broth supplemented with 100 μg/L ampicillin, which was then used to inoculate a 50 mL culture. After 1 h at 37 °C, expression was induced by addition of isopropyl-1-thio-D-galactopyranoside (IPTG) to a final concentration of 0.2 mM. Cells were allowed to grow for another 3 h at 30 °C and were then harvested by centrifugation and subsequently stored at −80 °C. For protein purification, 4 L of *E. coli* cells expressing pYcnD were grown in parallel and the resulting bacterial paste was resuspended in 50 mM sodium phosphate at pH 8.0 containing 300 mM sodium chloride and 10 mM imidazole (buffer A) as the resuspension buffer. Lysozyme was added to a final concentration of 1 mg/mL, and after 15 min at 4 °C, the cells were further lysed by sonication. The cell debris was removed by centrifugation at 25000*g* for 30 min at 4 °C, and the supernatant was subjected to affinity chromatography on Ni-NTA resin, essentially according to the protocol (number 11) provided by the supplier (Qiagen). In particular, buffer A containing 20 mM imidazole was used to wash the column and the bound protein was eluted in buffer A containing 150 mM imidazole. The progress of protein purification was monitored by 12.5% SDS−PAGE using the buffer system described by ref *10*.

The concentration of the YcnD preparation was determined spectrophotometrically at 450 nm using a molar extinction coefficient of $\epsilon_{450} = 12\,190\ M^{-1}\ cm^{-1}$ or with the Bradford reagent (Bio-Rad) using bovine serum albumin for calibration. The extinction coefficient for YcnD was calculated by recording differential spectra of the native and denatured protein, with the known extinction coefficient for authentic FMN being $\epsilon_{450} = 12\,500\ M^{-1}\ cm^{-1}$.

All fractions of high purity and an appropriate amount of enzyme (according to the SDS−PAGE) were pooled and concentrated by centrifugation with the Centriprep System from Amicon (molecular mass cutoff of 10 kDa). This system required repeated centrifugation at 1700*g* for 20 min at

4 °C (Hereaus Multifuge 3 S-R) until the final buffer [0.1 M Tris/HCl and 2 mM dithiothreitol (DTT) at pH 8.0] was added. Aliquots (1 mL) were stored at −20 °C.

Enzyme Assays. YcnD reductase activity was determined using either NADH or NADPH as the electron donor and various nitro compounds, chromate, and different azo dyes as electron acceptors. The reaction mixture consisted of 0.15 μM YcnD, 50 mM Tris/HCl (pH 8.0), and 0−364 μM NADH or 0−410 μM NADPH, respectively. The reaction mixture for the reduction of nitrofurazone consisted of 50 nM YcnD, 50 mM Tris/HCl (pH 8.0), 100 μM NADH, and 0−20 μM nitrofurazone and for the reduction of chromate of 0.15 μM YcnD, 50 mM Tris/HCl (pH 8.0), 250 μM NADH, and 0−50 μM potassium chromate. The reactions were initiated by the addition of NADH or NADPH, and the initial rate was measured with a Specord 205 spectrophotometer (Analytik Jena, Germany) at 25 °C using the following extinction coefficients: 6220 M^{-1} cm^{-1} for NAD(P)H at 340 nm and 8213 M^{-1} cm^{-1} for nitrofurazone at 410 nm.

Experiments with external FMN were carried out at concentrations of 1, 2, 3, 4, and 5 μM by addition of the appropriate volume of a FMN stock solution to mixtures of YcnD and NADH or NADPH. Again the reactions were started by the addition of 0−364 μM NADH and 0−410 μM NADPH, respectively, and the decrease in absorbance at 340 nm was monitored.

SDS−PAGE. Protein samples were separated by SDS−PAGE (12.5%) under reducing conditions as described by Laemmli (*10*). Gels were stained with Coomassie Brilliant Blue R or alternatively blotted onto nitrocellulose membranes.

Crystal Structure Analysis. Diffraction quality crystals of YcnD were obtained at room temperature using the vapor diffusion hanging drop method with 28% PEG 400, 0.2 M $CaCl_2$ in 0.1 M Na−HEPES buffer at pH 7.5 in the reservoir (100 μL), and with 1−2 μL drops consisting of the reservoir solution and a 10 mg/mL solution of the enzyme (in 100 mM Tris/HCl buffer at pH 8.5) in a 1:1 mixture.

Before flash freezing, crystals were soaked for about 30 s in a cryoprotectant, consisting of the reservoir solution plus 10% glycerol. A first complete dataset (YcnD1) extending to 2.05 Å was collected at cryogenic temperature on a rotating anode generator equipped with a MAR imaging plate. Subsequently, a higher resolution data set (YcnD2, 1.85 Å) was measured using synchrotron radiation at the EMBL/DESY in Hamburg (Table 3). In both cases, data reduction involved DENZO and SCALEPACK (*11*), as well as software from the CCP4 suite (*12*).

The structure was solved by molecular replacement with EPMR (*13*) using the YcnD1 dataset and the structure of the NADPH:FMN OR from *V. harveyi* (PDB entry: 1bkj) (*14*) as a search model (36% sequence identity to YcnD). All solvent and cofactor atoms were removed from the template structure, while the original side chains and *B* factors were retained. The EPMR calculations (50 independent runs for 50 generations each, with a population size of 600) yielded rather weak solutions with a maximum correlation coefficient of 0.266. On the basis of this initial phase information, the whole protein, except for six residues at the N terminus and the loop from 210 to 217, was rebuilt including all side chains in 200 cycles of automated model building using ARP/wARP (*15*) (20 autobuilding cycles including 10 cycles of model refinement, sequence docking after 12 autobuilding cycles, resolution range of 10−2.05 Å). The missing amino acids as well as the FMN cofactor could unambiguously be placed in the resulting clear difference electron density.

The structure was refined using CNS (*16*), and the required topology and parameter files for FMN were created using XPLO2D (*17*). Model building and fitting steps involved the graphics program O (*18*), using σ_A-weighted $2F_o - F_c$ and $F_o - F_c$ electron-density maps (*19*). R_{free} values (*20*) were computed from 5% randomly chosen reflections not used throughout the refinement. Water molecules were placed automatically into difference electron-density maps and were retained or rejected on the basis of geometric criteria as well as on their refined *B* factors ($B < 50$ Å^2). Two such water molecules were later reinterpreted as a chloride and a calcium ion based on unrealistically low refined *B* factors and on an analysis of the interactions with surrounding atoms. The hexa-His tag attached to the C terminus of the protein was not visible in the electron density. In the case of the high-resolution dataset YcnD2, alternate side-chain conformations were refined for Glu-20, Glu-32, Lys-59, Asp-71, Glu-147, Gln-203, Ser-205, and Lys-242. Root-mean-square deviations (RMSD values) from ideal values (*21*) were calculated as 0.006 Å for bond lengths, 1.1° for bond angles, and 22° for dihedral angles. All residues except one have their ϕ/ψ values in core and allowed regions of the Ramachandran plot. The only outlier (Glu-185) is located in a sharp turn and showed clear electron density and slightly lower than average *B* factors. Details of the data collection, processing, and structure refinement are summarized in Table 3. Structural representations shown in Figures 6, 8A, and 9 were prepared using PyMol (http://www.pymol.org).

RESULTS AND DISCUSSION

Heterologous expression of C-terminal hexa-histidine-tagged YcnD in *E. coli* could be achieved in good yield resulting in 20−25 mg of purified protein after Ni-NTA affinity chromatography from 10 g of wet biomass. The UV−vis absorbance spectrum of YcnD indicated the presence of a flavin chromophore with absorbance maxima at 370 and 450 nm with some resolution of the long-wavelength absorbance peak (Figure 1). The extinction coefficient of the YcnD-bound flavin was determined to be 12 190 M^{-1} cm^{-1} at 450 nm (see the Materials and Methods).

The viability of a *ycnD* deletion mutant suggests that the protein is not essential for *B. subtilis* under the conditions studied (http://bacillus.genome.jp). Because YcnD may supply reduced FMN to chorismate synthase, an enzyme involved in the biosynthesis of aromatic compounds, such as the aromatic amino acids, we have grown both the wild-type and the *ycnD* deletion mutant (YcnDd, kindly provided by Dr. Kobayashi, Nara, Japan) in medium lacking phenylalanine or tyrosine. In neither case could we observe any difference in the growth rate or behavior. This result does not necessarily exclude the involvement of YcnD in the generation of reduced FMN for chorismate synthase, because we currently do not know the expression pattern and function of YcnD homologues such as the closely related YwcG. To further evaluate the role of bacterial ORs, it appears necessary

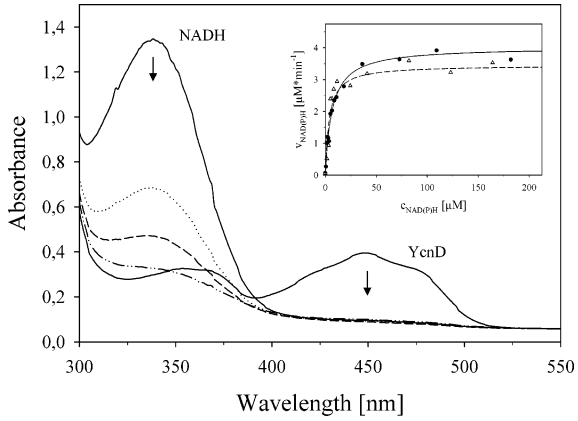

FIGURE 1: Reduction of YcnD with NADH in the presence of dissolved oxygen. The absorbance spectrum of YcnD (40 μM) in 50 mM Tris/HCl buffer (pH 8.0) was recorded at 25 °C. Reduction of YcnD-bound FMN was initiated by the addition of 400 μM NADH and was complete in less than 30 s. In the course of 10 min, residual NADH was fully oxidized (arrow on the left). Spectra recorded after 0, 30, 300, and 600 s (from top to bottom) are shown. The inset shows the Michaelis−Menten plots for the consumption of NADH (△) and NADPH (●) by YcnD.

to generate multiple gene deletions of enzymes that may have redundant physiological activities.

To characterize the putative OR activity of YcnD, reduced nicotinamide nucleotides (NADH and NADPH) were added to YcnD. As shown in Figure 1, YcnD was readily reduced by NADH as well as by NADPH as indicated by the complete loss of absorbance at 450 nm. The K_m values for NADH and NADPH were determined to be 6.4 and 4.4 μM, respectively. Under these *in vitro* aerobic conditions, excess NADH or NADPH is completely oxidized by the enzyme because of the reduction of dissolved dioxygen via the enzyme-bound flavin cofactor (Figure 1). The putative physiological electron acceptor is however another FMN molecule, which enters the active site of ORs to sequester the electron from enzyme-bound flavin. Therefore, this reaction was further analyzed by the addition of free FMN to reaction mixtures containing YcnD and varying concentrations of either NADH or NADPH. In the latter case, the initial velocity of NADPH oxidation as a function of the FMN concentration gives rise to a family of parallel lines (Figure 2A). This behavior was previously found for NfrA1 (YwcG), a *B. subtilis* homologue of YcnD, as well as other NAD(P)H:FMN ORs (*2*) and indicates a ping-pong Bi-Bi reaction mechanism. From the primary plot of data, a K_m of 6.3 μM is obtained for NADPH (slope divided by the intercept). A replot of the *y*-axis intercepts against the reciprocal FMN concentration yields a $K_m = 4.2$ μM for FMN and $V_{max} = 200$ μmol min^{-1} mg^{-1}. The K_m of NADPH is comparable to the one reported for other ORs, while V_{max} is about 20-times higher than the value measured for the homologous YwcG (*2*).

Interestingly, when NADH was used as the electron donor for YcnD, FMN showed an inhibitory effect on the observed initial velocities of oxidation (Figure 2B). The data indicate that FMN is a competitive inhibitor of NADH. Although the enzyme does not have a strong preference for either NADH or NADPH as indicated by the similarity of K_m values (see above), selective pressure is introduced by the presence of (oxidized) FMN, which inhibits the use of NADH and therefore leads to the preferential utilization of NADPH for

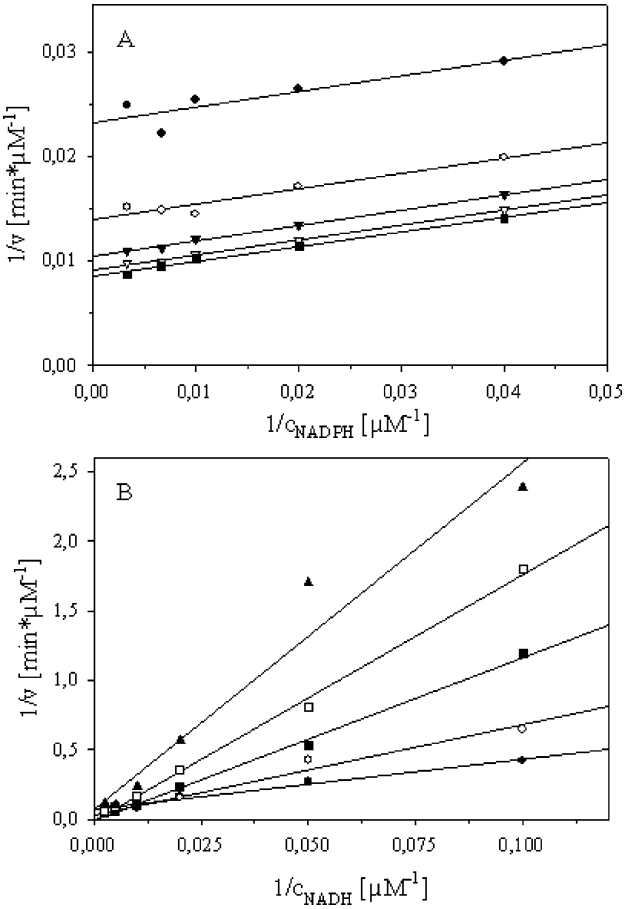

FIGURE 2: Determination of the reaction mechanism of YcnD with NADH and NADPH, respectively, in the presence of external FMN. (A) Double-reciprocal plot of the initial velocity of YcnD with NADPH in the presence of external FMN. The reaction mixture (1 mL) contained 0.15 μM YcnD in a 50 mM Tris/HCl buffer (pH 8.0), 0−410 μM NADPH, and constant amounts of FMN (1, 2, 3, 4, and 5 μM, respectively; from top to bottom). The reaction was initiated by the addition of NADPH. (B) Double-reciprocal plot of the initial velocity of YcnD with NADH in the presence of external FMN. The reaction mixture (1 mL) contained 0.15 μM YcnD in a 50 mM Tris/HCl buffer (pH 8.0), 0−364 μM NADH, and constant amounts of FMN (1, 2, 3, 4, and 5 μM, respectively; from bottom to top). The reaction was initiated by the addition of NADH.

the transfer of electrons to the FMN substrate. To our knowledge, this inhibitory behavior with regard to NADH has not been reported for other ORs thus far. On the basis of the terminology proposed by Tu (*4*), YcnD could be classified as a FRP, because NADPH is the preferred reductant in the presence of FMN as the electron acceptor.

Although the function of this family of bacterial ORs appears to be the generation of reduced FMN for the use in other enzymatic reactions, the enzymes were also reported to carry out a series of alternative reactions such as the reduction of nitro compounds and inorganic chromate (*2*, *22*, *23*). To test this ability for our recombinant YcnD, methyl-4-nitrobenzenesulfonate (NBS), 4-nitrophenol (NP), and 5-nitro-2-furaldehyde semicarbazone (nitrofurazone, NF) were analyzed. In all cases, YcnD was able to reduce the nitro compound, as exemplified for NBS and NF in Figure 3. Both compounds exhibited substrate inhibition at higher concentrations, and therefore, the data were fitted with a nonlinear hyperbolic equation (see the caption of Figure 3) to derive the kinetic parameters of the enzymatic reduction

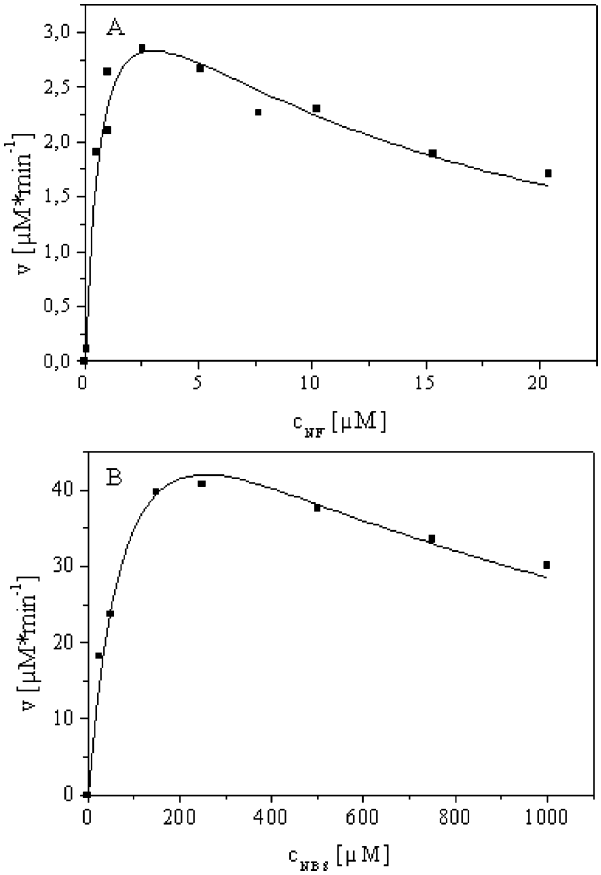

FIGURE 3: (A) Michaelis−Menten plot for the reduction of nitrofurazone (NF). The reaction mixture (1 mL) contained 50 nM YcnD in 50 mM Tris/HCl buffer (pH 8.0) and a constant amount of NADH (100 μM). The amount of substrate (NF) was varied from 0.1 to 20 μM. The reaction was initiated by the addition of NADH. The values for the initial reaction rate (V) were calculated using $V = \Delta c/\Delta t$ and plotted against the actual concentration of NF. A nonlinear hyperbolic curve fit for substrate inhibition was applied to obtain the kinetic parameters ($V_{max} = 4.1$ μM min^{-1}, $K_m = 0.7$ μM, and $K_i = 13$ μM). (B) Michaelis−Menten plot for the reduction of NBS. The reaction mixture (1 mL) contained 0.15 μM YcnD in a 50 mM Tris/HCl buffer (pH 8.0) and a constant amount of NADH (250 μM). The amount of substrate (NBS) was varied from 0 to 1000 μM. The reaction was initiated by the addition of NADH. The values for the initial reaction rate (V) were calculated using $V = \Delta c/\Delta t = \Delta E/\Delta t$ and plotted against the actual concentration of NBS. When a nonlinear hyperbolic curve fit was applied for substrate inhibition, the kinetic parameters could be directly determined from the regression data ($V_{max} = 74$ μM min^{-1}, $K_m = 96$ μM, and $K_i = 680$ μM).

Table 1: Kinetic Parameters for Nitro-organic Compounds and Chromate[a]

compound	V_{max}	K_m	k_{cat}/K_m	K_i
NBS	73.6	96	5	680
NF	4	0.7	7.6	13
NP	7	0.2	210	no
chromate (CrVI)	0.9	5	1.1	no

[a] V_{max} in μmol min^{-1}; K_m in μM; k_{cat}/K_m in min^{-1} μM; K_i in μM; no = not observed.

(summarized in Table 1). In addition to these nitro-organic compounds, chromate was also found to be a substrate for YcnD, albeit with comparatively poor catalytic parameters (see Table 1). Interestingly, these reduction reactions occur in the absence of external FMN and are therefore believed to require binding of these substrates in the active site of the OR. However, titration of YcnD with the nitro-organic compounds, shown to act as substrates, did not produce any spectral perturbations of the YcnD-bound flavin cofactor. In addition, attempts to cocrystallize YcnD with the nitro compounds or to soak protein crystals with solutions of the nitro compound were unsuccessful (see also below). On the other hand, when the course of NADH oxidation was monitored spectrophotometrically, it could be shown that NF is reduced preferentially and only after all of the NF has been consumed, NADH is used to reduce dissolved dioxygen (data not shown). This finding also suggests that reduction of nitro compounds takes place in the vicinity of the reduced flavin cofactor in the active site of YcnD. These observations are consistent with a ping-pong mechanism, where NADPH enters the active site to reduce the tightly bound flavin and dissociates with subsequent reoxidation of the flavin by a nitro-organic compound. This scenario is similar to the reaction mechanism with NADPH and FMN as outlined above (see Figure 2).

Table 2: Specific Activities of Azo Dye Reduction by YcnD

azo dye	specific activity (nmol min^{-1} mg^{-1})
Ethyl Red	260
Cibacron	390
Orange IV	90
Ponceau 2R	50
Sudan Black	5
Sudan Orange	150
Tartrazine	180
Toluidine Red	2

Table 3: Summary of Crystallographic Data

	YcnD1	YcnD2
X-ray source	rotating anode	EMBL-X13
wavelength (Å)	1.5417	0.8126
temperature (K)	100	
space group	$C222_1$	
cell parameters		
a (Å)	59.22	59.10
b (Å)	88.77	89.08
c (Å)	94.35	93.61
resolution range	25−2.05	18−1.85
outer shell	2.10−2.05	1.89−1.85
R_{sym}	0.080 (0.368)	0.045 (0.202)
$I/\sigma(I)$	33.8 (6.1)	47.0 (8.1)
completeness (%)	93.4 (75.3)	99.6 (95.9)
redundancy	9.5	7.0
unique reflections	15 103	21 381
R/R_{free} (%)	17.3/21.6	17.1/19.7
RMSD from ideality		
bond lengths (Å)	0.006	0.006
bond angles (deg)	1.1	1.1
dihedral angles (deg)	20.8	21.0
improper dihedrals (deg)	0.76	0.78
average *B* values		
protein	23.3	17.9
cofactor	16.0	15.3
water, ions	32.0	31.1
PDB accession code		1ZCH

In contrast to these reduction processes, azo dyes are reduced by bacterial ORs only in the presence of external FMN, indicating that azo dye reduction occurs outside the active site of the enzyme. We have analyzed several azo dyes as potential substrates for YcnD. In all cases analyzed, the reduction process was dependent upon the presence of additional free FMN, with an FMN concentration of ca. 10 μM being optimal for azo dye reduction. A summary of the

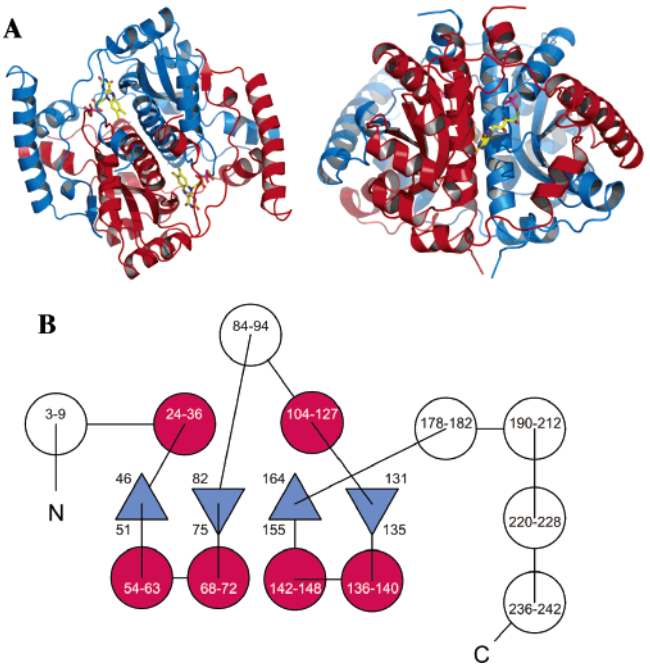

FIGURE 4: (A) Schematic ribbons representation of the YcnD−dimer generated by crystallographic 2-fold symmetry, viewed along (left) and perpendicular (right) to the symmetry axis. The FMN cofactor bound at the dimer interface is shown in yellow. (B) Topology diagram of YcnD.

rates determined for the reduction of several azo dyes is given in Table 2. The capacity of YcnD for azo dye reduction is in the same range as reported for the YcnD homologue NfrA1 from *B. subtilis* and NfsA from *E. coli (2, 23)*. On the other hand, these activities are 3 orders of magnitude lower than those found for bacterial azoreductases, which presumably bind the azo dye in the active site of the enzyme where reduction of the dye occurs (*24*, *25*). Our findings support the current model that azo dyes do not enter the active site of YcnD and that reduction of the azo dye is mediated by free reduced FMN, which in turn is generated by NADH/NADPH-dependent reduction in the active site of the enzyme.

To gain insight into the active-site architecture of the enzyme, we determined the X-ray crystal structure at 1.85 Å resolution. The overall fold of the protein is characterized by a three-layer αβα sandwich and strongly resembles folds from the NADH oxidase superfamily (CATH: 3.4.109.10) (*26*). The best match was found with the NADPH:FMN OR from *V. harveyi* (*14*) (1bjk, RMSD = 1.0 Å, 220-aligned Cα atoms) and the oxygen-insensitive nitroreductase NfsA from *E. coli* (*27*) (1f5v, RMSD = 1.2 Å, 228-aligned Cα atoms). Similar values for the RMSD (1.1−1.5 Å) but a lower fraction of aligned Cα atoms (140−160) were obtained when superimposing YcnD with the NADH oxidase from *Thermus thermophilus* (*28*) (1nox), the NAD(P)H:FMN OR from *Vibrio fischeri* (*29*) (1vfr), and the nitroreductases from *Enterobacter cloacae* (*30*) (1kqb) and *E. coli* (*31*) (1icu). In all of these cases, the closest similarities were observed for the αβα-sandwich core of the proteins and the location of the flavin cofactor (Figure 7).

The asymmetric unit contains one YcnD monomer, but a heavily intertwined homodimer (Figure 4) is generated through a crystallographic 2-fold symmetry axis parallel to *a* (x, $-y$, $-z$). In this dimer, a mostly helical domain extending from the αβα core of one subunit embraces the other monomer and more than 5000 Å^2 of mostly hydrophobic solvent-accessible surface become buried on each subunit upon dimer formation. Two salt bridges (Arg-56−Glu-185 and Glu-105−Arg-139) are located at the interface, with the latter being almost completely buried. An additional link between the monomers is formed by a calcium ion ligated to the side chains of Glu-150 and Asn-189 (from the symmetry-related protein chain).

The amount of buried surface area is among the largest found thus far for homodimeric proteins (*32*), and comparable values can be calculated for the structures of the *V. harveyi* OR and *E. coli* NfsA. These data strongly suggest that the dimer of YcnD is the physiological unit of the enzyme. Interestingly, a monomer/dimer equilibrium has been observed for the homologous OR from *V. harveyi*, and only the monomeric form of this enzyme was shown to form a complex with luciferase, supposedly facilitating the channeling of reduced FMN that is required for the luciferase reaction (*4*, *5*). The structural data (indicating an exceptionally strong interaction between the subunits) seem to contradict these findings, although it has to be noted that the conditions during crystallization were markedly different from those used in the binding experiments.

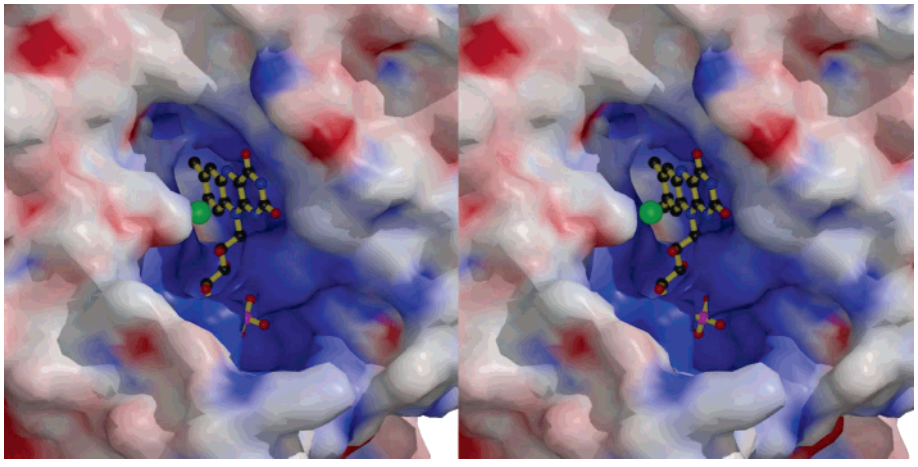

FIGURE 5: Surface representation of the FMN-binding site of YcnD. The molecular surface is colored according to the electrostatic potential (blue and red shades denoting positive and negative potentials) as calculated using Grasp (*38*). This figure was prepared using Molscript (*39*) and Raster3D (*40*).

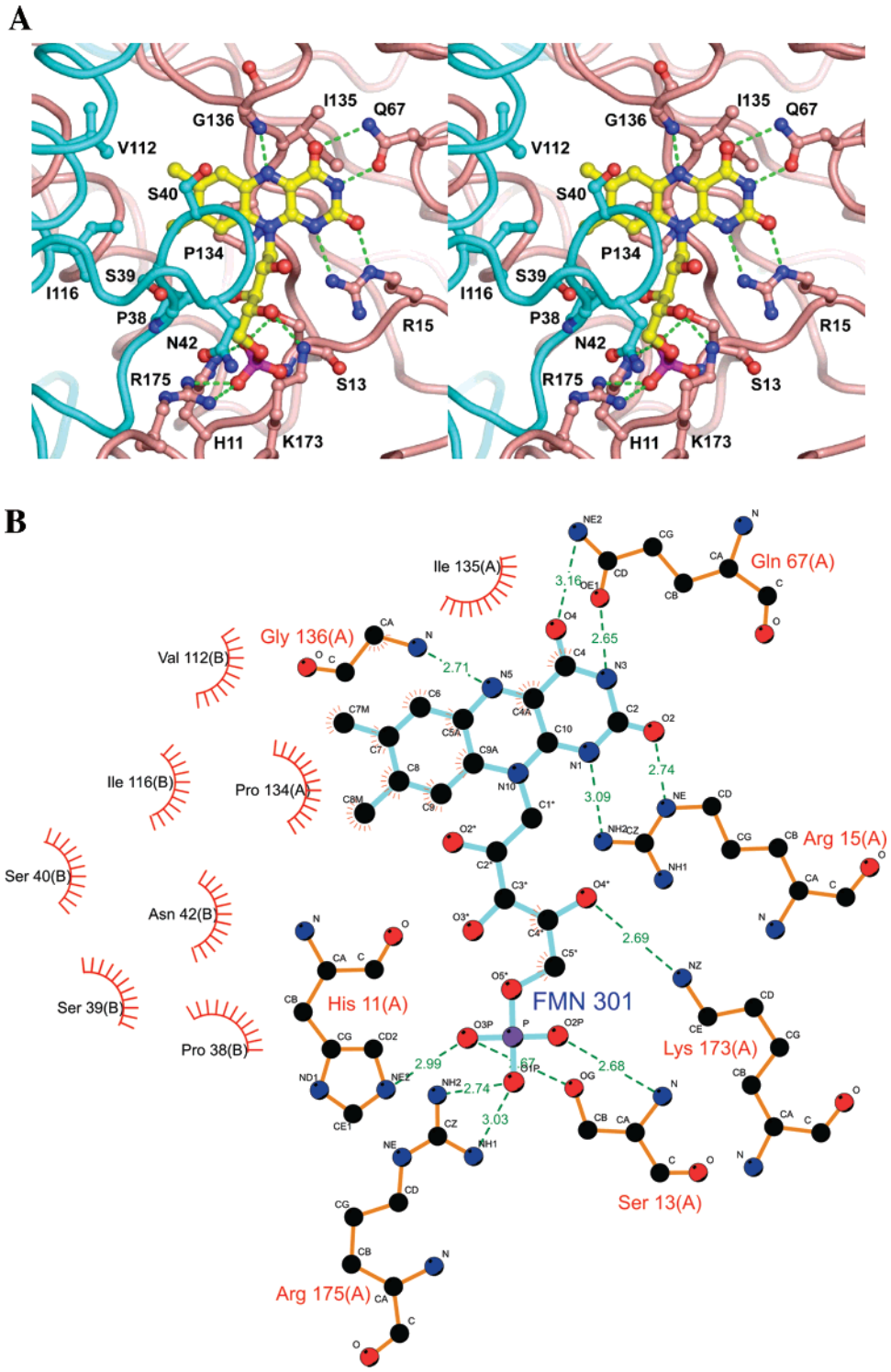

FIGURE 6: Close-up of the active site of YcnD (A) and schematic LigPlot representation (*41*) of the interaction of FMN with surrounding amino acid residues (B). The two chains of the YcnD dimer are shown in pink and light blue, with the cofactor in yellow. Nitrogen and oxygen atoms are drawn in blue and red, respectively, and hydrogen-bonding interactions are depicted as green dashed lines.

With respect to the calcium ion bound at the YcnD−dimer interface, it is tempting to hypothesize that calcium binding is involved in stabilizing the dimer and that changes in the calcium concentration (or of another divalent metal cation) can modulate the stability of the complex under physiological conditions. In the hitherto reported structures of related ORs, no such cation binding has been identified. The ligation site observed in YcnD, however, is located at the very periphery of the dimer interface at the surface of the protein with the first coordination sphere including a glutamic acid side chain (Glu-25) from a third symmetry-related chain. Given the high concentration of calcium (i.e., 0.2 M) in the crystallization buffer, a genuine physiological role of this cation-mediated interaction appears less likely. On the other hand, a possible role of this site in regulating the dimerization of YcnD and of homologous ORs remains an interesting mechanism for regulating the monomer−dimer equilibrium of the enzyme. Such a mechanism may be especially important for the

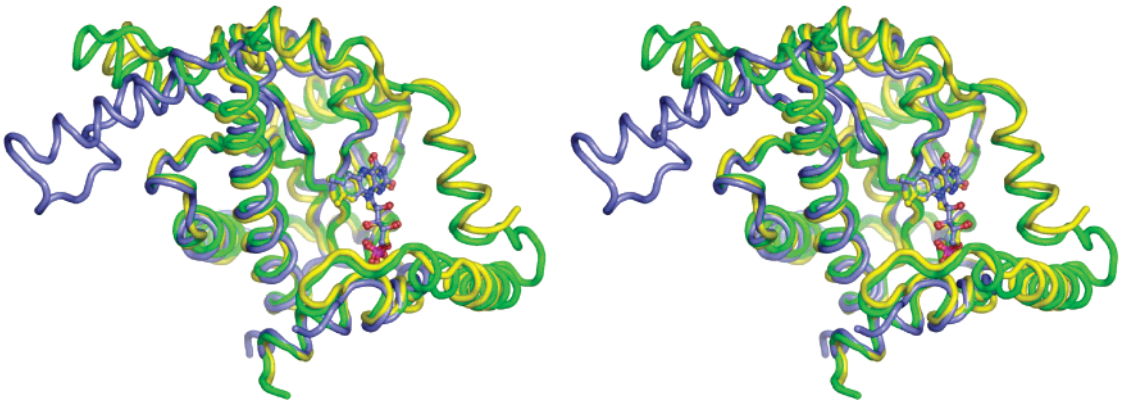

FIGURE 7: Stereorepresentation of the superposition of YcnD (green) with the NADPH:FMN OR from *V. harveyi* (yellow, refcode: 1bkj) (*14*) and the NADH oxidase from *Thermus thermophilus* (blue, refcode: 1nox) (*28*). All three proteins are dimers, of which only the monomers are shown together with one FMN cofactor molecule.

formation of protein complexes between the OR and acceptor proteins for reduced FMN, such as demonstrated for the bacterial luciferase (*5*).

The FMN is bound at the dimer interface in a deep crevice, leaving only the *re* face accessible to the substrate. The cofactor-binding site is composed of residues from both subunits and exhibits a predominantly positive electrostatic potential (Figure 5). Of the two subunits, one is mainly involved in polar interactions, while the other forms a hydrophobic pocket occupied by the dimethylbenzene portion of the cofactor (Figure 6). The isoalloxazine moiety is slightly bent with a butterfly angle around the N5−N10 axis of 8.8°. An arginine residue (Arg-15) is interacting with the N1−C2−O2 portion of the cofactor, and Gly-136 forms a hydrogen bond to N5. In addition, the carboxamide group of Gln-67 is hydrogen-bonded to O4 and N3 of FMN. The negative charge of the terminal phosphate group is complemented by the positive charges of Arg-175, Lys-173, and His-11. The positive charge close to the N1−C2−O2 locus is found (in differing manifestations) in many flavin-containing enzymes (*33*). It is supposed to raise the redox potential of the cofactor and to increase its binding affinity to the enzyme (*33*, *34*). A hydrogen-bonding donor close to N5 is also a rather common feature in flavoenzymes and may play an additional role in the fine-tuning of the redox potential. All residues involved in interactions with the phosphate group of the cofactor are conserved among YcnD, the OR from *V. harveyi*, and NfsA from *E. coli*. The general pattern of interactions with the isoalloxazine moiety and the residues Arg-15, Gln-67, and Gly-136 are also conserved among the three proteins. The same is true for the accessibility of the flavin, suggesting N5 to be the likely candidate for accepting a hydride from NAD(P)H.

A chloride ion is bound close to the cofactor (Figure 5), accepting hydrogen bonds from the main-chain amide group of Ile-41 (second chain), the O2′ hydroxyl group of FMN, and a water molecule. At the analogous position, a phosphate ion was observed in the structure of the *V. harveyi* OR (*14*). In the complex of the same enzyme with NAD^+ (*35*), the diphosphate moiety of the bound nucleotide is also located in this region. In addition, the carboxyl groups of acetate and benzoate ions were observed at this position in structures of the nitroreductase from *E. cloacae* (*30*). For structural reasons, it appears unlikely that this anion-binding site houses the pyrophosphate (or the 2′-phosphate group) in a productive complex with NAD(P)H. However, it was suggested as the site for the "initial landing" of NAD(P)H followed by a subsequent repositioning (*14*). In the structure of the *V. harveyi* enzyme, the hydroxyl group of Ser-41 forms a hydrogen bond with the bound phosphate. This residue is replaced by an isoleucine in YcnD; its role, however, could be taken by the neighboring Ser-40 (Figure 6).

Preliminary visual docking of NBS and NF suggested that the active site of YcnD is spacious enough to accept these substrates. Although the binding site is apparently accessible in the crystal lattice, soaking experiments with these substances have thus far been unsuccessful, possibly because of their rather low solubility. In addition, crystallization trials in the presence of the substrates, 4-nitrophenol or FMN, did not yield crystals. In the absence of structural information on enzyme substrate complexes, one can only speculate about possible roles of active-site residues. As indicated above, the hydroxyl group of Ser-40, the main-chain amide of Ile-41, and the O2′ of FMN are very likely involved in substrate binding through the formation of hydrogen bonds. In crystal structures of complexes of a structurally related *E. coli* nitroreductase with prodrug molecules, the nitro group that is reduced by this enzyme was also found to interact with the equivalent residues (*36*). Another feature of the active site, which sets YcnD apart from the other structurally characterized ORs, is the presence of four tyrosine residues (Tyr-227, Tyr-228, Tyr-232, and Tyr-233), which may also interact with the substrate via hydrogen bonds or aromatic stacking interactions.

Mutagenesis data obtained with an oxidoreductase (FRP) from *V. harveyi* and NfsA from *E. coli* indicated that Arg-203 (*E. coli* numbering) plays a crucial role in binding and recognition of NADPH and is involved in interactions with its 2′-phosphate group (*27*, *33*, *37*). The structurally corresponding residue in YcnD, Arg-211, is part of a loop structure at the periphery of the protein. Atoms in this region showed high *B* factors in the crystallographic refinement of both structures. Similarly, the corresponding region around the conserved Arg-203 in the OR from *V. harveyi* was not visible at all in electron-density maps (*14*). These observations indicate a pronounced flexibility of this part of the OR structure. Indeed, modeling of the NfsA NAPDH complex suggests conformational flexibility of the protein to be necessary for NADPH binding (*27*).

The present biochemical and structural work has set the stage for further investigations of the role of ORs in *B. subtilis*. With regard to YcnD, functional analysis will focus on the identification of acceptor enzymes that form protein complexes similar to those identified in the bacterial luciferase system (*5*). Toward this goal, we will study putative interactions of YcnD with monofunctional flavin-dependent hydroxylases and of chorismate synthase. In this context, it is interesting to note that *Saccharomyces cerevisiae* does not possess a YcnD or YwcG homologue. The lack of these ORs in yeast is matched by the occurrence of a bifunctional chorismate synthase, which is able to utilize NAD(P)H directly to reduce the FMN cofactor to its active redox state. Hence, it can be speculated that yeast enzymes do not rely on the provision of the reduced flavin cofactor because they have an intrinsic ability to carry out this reaction.

ACKNOWLEDGMENT

X-ray diffraction data were collected at the EMBL beamline X13 (c/o DESY, Hamburg, Germany). We are especially indebted to Andrea Schmidt for her help in data collection.

REFERENCES

1. Kunst, F., Ogasawara, N., Moszer, I., Albertini, A. M., Alloni, G., Azevedo, V., Bertero, M. G., Bessieres, P., Bolotin, A., Borchert, S., Borriss, R., Boursier, L., Brans, A., Braun, M., Brignell, S. C., Bron, S., Brouillet, S., Bruschi, C. V., Caldwell, B., Capuano, V., Carter, N. M., Choi, S. K., Codani, J. J., Connerton, I. F., Danchin, A., et al. (1997) The complete genome sequence of the gram-positive bacterium *Bacillus subtilis*, *Nature 390*, 249−256.
2. Zenno, S., Kobori, T., Tanokura, M., and Saigo, K. (1998) Purification and characterization of NfrA1, a *Bacillus subtilis* Nitro/flavin reductase capable of interacting with the bacterial luciferase, *Biosci. Biotechnol. Biochem. 62*, 1978−1987.
3. Fontecave, M., Eliasson, R., and Reichard, P. (1987) NAD(P)H: flavin oxidoreductase of *Escherichia coli*. A ferric iron reductase participating in the generation of the free radical of ribonucleotide reductase, *J. Biol. Chem. 262*, 12325−12331.
4. Tu, S.-C. (2001) Reduced flavin: Donor and acceptor enzymes and mechanisms of channeling, *Antioxid. Redox Signaling 3*, 881−897.
5. Jeffers, C. E., Nichols, J. C., and Tu, S.-C. (2003) Complex formation between *Vibrio harveyi* luciferase and monomeric NADPH:FMN oxidoreductase, *Biochemistry 42*, 529−534.
6. Sancar, G. B., Jorns, M. S., Payne, G., Fluke, D. J., Rupert, C. S., and Sancar, A. (1987) Action mechanism of *Escherichia coli* DNA photolyase. III. Photolysis of the enyzme−substrate complex and the absolute action spectrum, *J. Biol. Chem. 262*, 492−498.
7. Macheroux, P., Schmid, J., Amrhein, N., and Schaller, A. (1999) A unique reaction in a common pathway: Mechanism and function of chorismate synthase in the shikimate pathway, *Planta 207*, 325−334.
8. Hasan, N., and Nester, E. W. (1978) Purification and characterization of NADPH-dependent flavin reductase. An enzyme required for the activation of chorismate synthase in *Bacillus subtilis*, *J. Biol. Chem. 253*, 4987−4992.
9. Fitzpatrick, T. B., Amrhein, N., and Macheroux, P. (2003) Characterization of YqjM, an old yellow enzyme homolog from *Bacillus subtilis*, *J. Biol. Chem. 278*, 19891−19897.
10. Laemmli, U. K. (1970) Cleavage of structural proteins during the assembly of the head of bacteriophage T4, *Nature 227*, 680−685.
11. Otwinowski, Z., and Minor, W. (1997) Processing of X-ray diffraction data collected in oscillation mode, *Methods Enzymol. 276*, 307−326.
12. CCP4 (1994) The CCP4 suite−Programs for protein crystallography, *Acta Crystallogr., Sect. D: Biol. Crystallogr. 50*, 760−763.
13. Kissinger, C. R., Gehlhaar, D. K., and Fogel, D. B. (1999) Rapid automated molecular replacement by evolutionary search, *Acta Crystallogr., Sect. D: Biol. Crystallogr. 55*, 484−491.
14. Tanner, J. J., Lei, B., Tu, S.-C., and Krause, K. L. (1996) Flavin reductase P: structure of a dimeric enzyme that reduces flavin, *Biochemistry 35*, 13531−13539.
15. Morris, R. J., Perrakis, A., and Lamzin, V. S. (2003) ARP/wARP and automatic interpretation of protein electron density maps, *Methods Enzymol. 374*, 229−244.
16. Brünger, A. T., Adams, P. D., Clore, G. M., Delano, W. L., Gros, P., Grosse-Kunstleve, R. W., Jiang, J. S., and Warren, G. L. (1998) Crystallography and NMR system (CNS): A software system for macromolecular structure determination, *Acta Crystallogr., Sect. D: Biol. Crystallogr. 54*, 905−921.
17. Kleywegt, G. J., and Jones, T. A. (1997) Model-building and refinement practice, *Methods Enzymol. 277*, 208−230.
18. Jones, T. A., Zou, J. Y., Cowan, S., and Kjeldgaard, M. (1991) Improved methods for building protein models in electron density maps and the location of errors in these models, *Acta Crystallogr., Sect. A: Found. Crystallogr. 47*, 110−119.
19. Read, R. J. (1986) Improved Fourier coefficients for maps using phases from partial structures with errors, *Acta Crystallogr., Sect. A: Found. Crystallogr. 42*, 140−149.
20. Kleywegt, G. J., and Brunger, A. T. (1996) Checking your imagination−Applications of the free *R*-value, *Structure 4*, 897−904.
21. Engh, R. A., and Huber, R. (1991) Accurate bond and angle parameters for X-ray protein structure refinement, *Acta Crystallogr., Sect. A: Found. Crystallogr. 47*, 392−400.
22. Kwak, Y. H., Lee, D. S., and Kim, H. B. (2003) *Vibrio harveyi* nitroreductase is also a chromate reductase, *Appl. Environ. Microbiol. 69*, 4390−4395.
23. Zenno, S., Koike, H., Kumar, A. N., Jayaraman, R., Tanokura, M., and Saigo, K. (1996) Biochemical characterization of NfsA, the *Escherichia coli* major nitroreductase exhibiting a high amino acid sequence homology to Frp, a *Vibrio harveyi* flavin oxidoreductase, *J. Bacteriol. 178*, 4508−4514.
24. Nakanishi, M., Yatome, C., Ishida, N., and Kitade, Y. (2001) Putative ACP phosphodiesterase gene (acpD) encodes an azoreductase, *J. Biol. Chem. 276*, 46394−46399.
25. Suzuki, Y., Yoda, T., Ruhul, A., and Sugiura, W. (2001) Molecular cloning and characterisation of the gene coding for azoreductase from *Bacillus* sp. OY1-2 isolated from soil, *J. Biol. Chem. 276*, 9059−9065.
26. Orengo, C. A., Michie, A. D., Jones, S., Jones, D. T., Swindells, M. B., and Thornton, J. M. (1997) CATH−A hierarchic classification of protein domain structures, *Structure 5*, 1093−1108.
27. Kobori, T., Sasaki, H., Lee, W. C., Zenno, S., Saigo, K., Murphy, M. E. P., and Tanokura, M. (2001) Structure and site-directed mutagenesis of a flavoprotein from *Escherichia coli* that reduces nitrocompounds: Alteration of pyridine nucleotide binding by a single amino acid substitution, *J. Biol. Chem. 276*, 2816−2823.
28. Hecht, H. J., Erdmann, H., Park, H. J., Sprinzl, M., and Schmid, R. D. (1995) Crystal structure of NADH oxidase from *Thermus thermophilus*, *Nat. Struct. Biol. 2*, 109−114.
29. Koike, H., Sasaki, H., Kobori, T., Zenno, S., Saigo, K., Murphy, M. E. P., Adman, E. T., and Tanokura, M. (1998) 1.8 Å crystal structure of the major NAD(P)H:FMN oxidoreductase of a bioluminescent bacterium, *Vibrio fischeri*: Overall structure, cofactor, and substrate-analog binding, and comparison with related flavoproteins, *J. Mol. Biol. 280*, 259−273.
30. Haynes, C. A., Koder, R. L., Miller, A.-F., and Rodgers, D. W. (2002) Structures of nitroreductase in three states. Effects of inhibitor binding and reduction, *J. Biol. Chem. 277*, 11513−11520.
31. Lovering, A. L., Hyde, E. I., Searle, P. F., and White, S. A. (2001) The structure of *Escherichia coli* nitroreductase complexed with nicotinic acid: Three crystal forms at 1.7, 1.8, and 2.4 Å resolution, *J. Mol. Biol. 309*, 203−213.
32. Ponstingl, H., Henrick, K., and Thornton, J. M. (2000) Discriminating between homodimeric and monomeric proteins in the crystalline state, *Proteins 41*, 47−57.
33. Fraaije, M. W., and Mattevi, A. (2000) Flavoenzymes: Diverse catalysts with recurrent features, *Trends Biochem. Sci. 25*, 126−132.
34. Ghisla, S., and Massey, V. (1989) Mechanisms of flavoprotein-catalyzed reactions, *Eur. J. Biochem. 181*, 1−17.

35. Tanner, J. J., Tu, S.-C., Barbour, L. J., Barnes, C. L., and Krause, K. L. (1999) Unusual folded conformation of nicotinamide adenine dinucleotide bound to flavin reductase P, *Protein Sci. 8*, 1725−1732.
36. Johansson, E., Parkinson, G. N., Denny, W. A., and Neidle, S. (2003) Studies on the nitroreductase prodrug-activating system. Crystal structures of complexes with the inhibitor dicoumarol and dinitrobenzamide prodrugs and of the enzyme active form, *J. Med. Chem. 46*, 4009−4020.
37. Wang, H., Lei, B., and Tu, S.-C. (2000) *Vibrio harveyi* NADPH−FMN oxidoreductase Arg203 as a critical residue for NADPH recognition and binding, *Biochemistry 39*, 7813−7819.
38. Nicholls, A. J. (1993) Columbia University, New York.
39. Kraulis, P. J. (1991) MOLSCRIPT: A program to produce both detailed and schematic plots of protein structures, *J. Appl. Crystallogr. 24*, 946−950.
40. Merritt, E. A., and Bacon, D. J. (1997) Raster3D: Photorealistic molecular graphics, *Methods Enzymol. 277*, 505−524.
41. Wallace, A. C., Laskowski, R. A., and Thornton, J. M. (1995) LIGPLOT: A program to generate schematic diagrams of protein−ligand interactions, *Protein Eng. 8*, 127−134.

BI0510835